Jerzy GOŁĘBIOWSKI, Jarosław FORENC

Politechnika Białostocka, Wydział Elektryczny

doi:10.15199/48.2016.12.68

The influence of side thermal insulation on distribution of the temperature field in an electrical floor heater

Abstract. *Two models of side thermal insulation (adiabatic and lossy) were examined in the analysis of the operation of electrical floor heater. Temperature field distributions obtained in both cases were compared. Computation costs of consideration of edge effects resulted from insulation lossiness were estimated. The use of parallel operation of a traditional processor (CPU) and a graphics processing unit (GPU) enabled a significant reduction of the computation time.*

Streszczenie*. W analizie pracy elektrycznego grzejnika podłogowego rozpatrywano dwa modele bocznej izolacji termicznej (idealnej i rzeczywistej). Porównano rozkłady pola temperatury wyznaczone w wymienionych przypadkach. Oszacowano obliczeniowe koszty uwzględnienia efektów krawędziowych spowodowanych stratnością izolacji. Zastosowanie równoległej pracy tradycyjnego procesora (CPU) oraz procesora karty graficznej (GPU) umożliwiło znaczne skrócenie czasu obliczeń numerycznych. (****Wpływ bocznej izolacji termicznej na rozkład pola temperatury w elektrycznym grzejniku podłogowym****)*

Keywords: electric floor heating, transient temperature field, lossy thermal insulation, parallel computations, GPGPU
Słowa kluczowe: elektryczne ogrzewanie podłogowe, nieustalone pole temperatury, stratna izolacja termiczna, obliczenia równoległe, GPGPU.

Introduction

Numerical simulations are very important in the analysis of physical phenomena. Among others, they enable the analysis of complex problems without analytical solution or with analytical solution that is difficult to obtain. Numerical simulations also limit the necessity to build expensive prototypes and experiment with them [1]. Carrying out numerical simulations requires the development of an appropriate mathematical model of analysed phenomenon. This model should reflect reality as much as possible and, at the same time, it should allow obtaining results of the simulation within a reasonable time. For this reason, practical models are often applied with simplifying assumptions that reduce the cost of obtaining numerical solutions. Such a problem can be seen, among others, in the analysis of thermal phenomena occurring in floor heating systems [2, 3]. Electrical, water and air floor heaters share a similar construction [3]. Essential part of a floor heater is a layer of concrete slab, in which pipes, ducts or heating cables are placed. Half of an electrical floor heater is presented in Fig. 1. Basic thermal insulation is located under the concrete slab. Concrete base is the lowest layer. Floor covering or dry-set-mortar with flooring is placed on the upper surface of the heater. Additional side thermal insulation is placed on outer vertical edges of the concrete slab.

A few simplifying assumptions are applied in modelling of a floor heater. In most cases, the system is analysed as plane-parallel (two-dimensional) [4-9]. It significantly reduces the size of a model and, at the same time, shortens the numerical computations time. Ideal (adiabatic) side insulation is mostly assumed on outer vertical concrete slab walls. Thanks to this assumption, the distribution of a temperature field in the heater is repeatable and the analysis can be limited to an area placed between two heat sources [5-7] or to half of this area [4, 8, 9]. In some cases, perfect basic thermal insulation (on the bottom surface of a floor slab) is also assumed [5, 9]. This assumption reduces the number of the layers of heating system.

Side thermal insulation closer to reality may be also analysed at outermost vertical walls of the concrete slab (Fig. 1). Therefore, the primary purpose of this paper is the examination of the impact of side insulation lossiness on the simulated temperature field distribution of the heating system. Two-dimensional initial-boundary value problem of heat equation was formulated for a model with lossy insulation on vertical walls of the concrete slab. This problem was discretized with the implicit finite difference method. Obtained system of algebraic equations was solved on a traditional processor (CPU) and graphics processing unit (GPU). Simultaneous (parallel) work of these processors enables a significant reduction of the time of computations (what should be considered as the second purpose of this paper). In the analysis Biconjugate Gradient Stabilized method (BiCGStab) [10-12] with Jacobi preconditioner [11, 12] was used. Results of computations in the form of profiles and distributions of temperature field

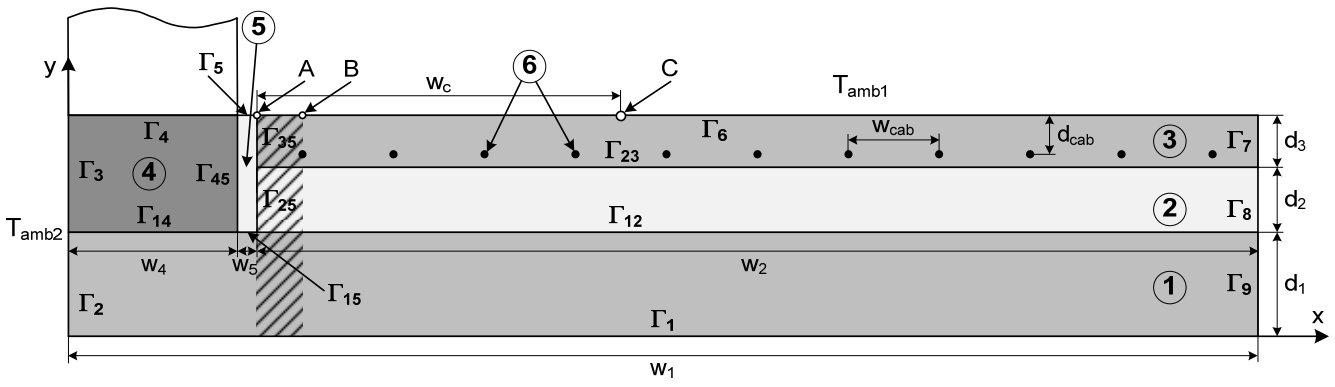

Fig.1. Half of the cross-section of electrically heated floor: 1 - concrete base, 2 - basic thermal insulation, 3 - concrete slab, 4 - outer wall, 5 - side thermal insulation, 6 - heating cables

were compared with solutions of a model with perfect (adiabatic) insulation of vertical walls of the concrete slab.

Mathematical model of a floor heater

In the system with ideal side thermal insulation, analysis of the thermal field distribution in a cross-section of a heater may be limited to hatched area shown in Fig. 1. Appropriate initial-boundary value problem describing this case and its solution are presented in paper [13].

In case of lossy side thermal insulation model, external wall (area number 4 in Fig. 1) has to be taken into consideration because it has an influence on the temperature field distribution in the section of a heater.

In defined model it was assumed that the length of the system is much greater than its cross-sectional dimensions (like for example in long corridors, garden tunnels, circulation areas, etc). In this case the thermal field distribution can be discussed as a plain-parallel and it can be described by the two-dimensional heat equation [14]:

$$(1)\quad \frac{\partial^2 T_i(x,y,t)}{\partial x^2}+\frac{\partial^2 T_i(x,y,t)}{\partial y^2}-\frac{1}{\chi_i}\frac{\partial T_i(x,y,t)}{\partial t}=-\frac{g_i(x,y,t)}{\lambda_i}.$$

In equation mentioned above $T_i(x,y,t)$ describes temperature field of point at coordinates (x,y) in t time. Subscript i ($i = 1,2,...,5$) defines the material corresponding to a given point (Fig. 1). Next, $g_i(x,y,t)$ is the volumetric efficiency of heat sources (W/m^3). Thermal diffusivity of the ith material is defined by the following relationship:

$$(2)\quad \chi_i=\frac{\lambda_i}{c_i\rho_i},$$

where: λ_i - thermal conductivity, c_i - specific heat, ρ_i - mass density. These values are not dependent on the temperature. Such an assumption is valid because of the small range of temperature variations of the system. Parameters of the materials of zones (1 and 3) as well as (2 and 5) are equal in pairs.

In the analysed model it is assumed that identical outer walls are placed on the left and on the right side of the floor. What is more, it is assumed that the heating cable is arranged symmetrically with respect to a vertical line passing through the centre of the system ($x = w_1$). In order to ensure conditions appropriate for comparison of analysed systems, the first section of the cable was placed at a distance equal to half of the distance between heat sources (measuring from insulation).

The above discussion leads to the following condition:

$$(3)\quad \left.\frac{\partial T_i(x,y,t)}{\partial x}\right|_{x=w_1}=0 \quad for \quad y\in \Gamma_7\cup\Gamma_8\cup\Gamma_9,\ t\geq 0.$$

Temperature distribution is therefore symmetrical with respect to the centre of the floor and analysis can be limited to only half of the cross-section of the floor shown in Fig. 1.

The upper surface of the floor emits heat into the room by means of radiation and natural convection. This phenomenon is described by the III-rd kind boundary condition with the total heat transfer coefficient α_1:

$$(4)\quad -\lambda_i\left.\frac{\partial T_i(x,y,t)}{\partial y}\right|_{y=d}=\alpha_1\cdot\left[T_i(x,y=d,t)-T_{amb1}\right],$$

where: $d=d_1+d_2+d_3$,

$$\begin{cases} x\in\Gamma_5 & for\ i=5\\ x\in\Gamma_6 & for\ i=3\end{cases},\ t\geq 0,$$

T_{amb1} - an ambient room temperature.

Hankel's boundary condition was also put for an outer wall of a building (contour Γ_3) and for a concrete base (contour Γ_2):

$$(5)\quad \lambda_i\left.\frac{\partial T_i(x,y,t)}{\partial x}\right|_{x=0}=\alpha_2\cdot\left[T_i(x=0,y,t)-T_{amb2}\right],$$

where: $\begin{cases} x\in\Gamma_2 & for\ i=1\\ x\in\Gamma_3 & for\ i=4\end{cases},\ t\geq 0,$

α_2 - a total heat transfer coefficient,

T_{amb2} - a temperature outside of the building.

Horizontal cross-section of the outer wall on the level of the floor (Γ_4) is only 6.02% of the total perimeter of the system (Fig. 1). Furthermore, Γ_4 is located behind the thermal insulation 5. Therefore, heat transfer on Γ_4 is small and can be ignored:

$$(6)\quad \left.\frac{\partial T_4(x,y,t)}{\partial y}\right|_{y=d_1+d_2+d_3}=0 \quad for \quad x\in\Gamma_4,\ t\geq 0.$$

On the lower surface of the concrete base (contour Γ_1) a constant ground temperature (T_g) is assumed:

$$(7)\quad T_1(x,y=0,t)=T_g \quad for \quad x\in\Gamma_1,\ t\geq 0.$$

On the boundary contours Γ_{qr} (between qth and rth material zone) the conditions of the continuity of temperature and heat flux are met:

$$(8)\quad T_q(\Gamma_{qr},t)=T_r(\Gamma_{qr},t),$$

$$(9)\quad \lambda_q\left.\frac{\partial T_q(x,y,t)}{\partial \eta_{qr}}\right|_{\Gamma_{qr}}=\lambda_r\left.\frac{\partial T_r(x,y,t)}{\partial \eta_{qr}}\right|_{\Gamma_{qr}} \quad for \quad t\geq 0,$$

where pairs of indexes have the following values: ($q=1$, $r=2$), ($q=1$, $r=4$), ($q=1$, $r=5$), ($q=2$, $r=3$), ($q=2$, $r=5$), ($q=3$, $r=5$) and ($q=4$, $r=5$). $\partial(\ldots)/\partial\eta_{qr}$ defines derivatives normal to Γ_{qr} contour in points $(x,y)\in\Gamma_{qr}$.

Due to low cable mass (in comparison with the mass of the concrete) and small cable diameter (compared to the size of the intersection of the heater) the structure of a cable and temperature field of its intersection is not taken into consideration during the analysis. The heating cable is modelled with control surface S_{cab} which is a small surroundings of the cable axis. Volumetric efficiency of heat sources in points of a model that do not belong to control surface is zero. Heater is regulated by an on/off controller working with a temperature sensor. The sensor is located on the floor surface between two sections of a heating cable (point C in Fig. 1). When the temperature of the sensor point reaches T_{OFF} value, power supply of a heating cable is switched off and volumetric heat efficiency of surface control points of the cable is zero. On the other hand, when the temperature detected by the sensor is lower than T_{ON}, the power supply of a heating cable is switched on again and volumetric heat efficiency of the heat source is g_{cab}. The following relationships can be derived from these

assumptions:

(10a) $$g_1 = g_2 = g_4 = g_5 = 0,$$

(10b)
$$g_3(x,y,t) = \begin{cases} 0 \ \ for \ \ (x,y) \in S_{cab} \cap T_3(C,t) \geq T_{OFF} \cap \dfrac{\partial T_3(C,t)}{\partial t} > 0 \\ g_{cab} \ for \ \ (x,y) \in S_{cab} \cap \\ \qquad \left[t = 0 \cup \left\{ T_3(C,t) \leq T_{ON} \cap \dfrac{\partial T_3(C,t)}{\partial t} < 0 \right\} \right] \\ 0 \ \ for \ \ (x,y) \notin S_{cab} \end{cases}$$

Signs of derivatives found in (10b) clearly define moments of switching power supply of a heating cable off and on (accordingly, when sensor temperature is increasing and decreasing). The need for uniformization results from bilateral overshot beyond the range $\langle T_{ON}, T_{OFF} \rangle$ caused by thermal inertia of the system.

Initially $(t = 0)$ the system is in a steady state. Two-dimensional stationary heat equation has to be solved in order to determine temperatures in all points of the model in this state [14]:

(11) $$\frac{\partial^2 T_{ui}(x,y)}{\partial x^2} + \frac{\partial^2 T_{ui}(x,y)}{\partial y^2} = 0,$$

with similar boundary conditions (3)-(9) as in the case of equation (1). In above-mentioned conditions, temperature $T_i(x,y,t)$ should be replaced by temperature $T_{ui}(x,y)$. Furthermore, because of the opposite sense of the heat flow, left sides of equations (4) and (5) will change their signs. Solution of equation (11) uniformized this way is an initial condition for equation (1):

(12) $$T_i(x,y,t=0) = T_{ui}(x,y).$$

Equations (1)-(10) and (12) define initial-boundary value problem. Solution of this problem models functioning of a floor heater with lossy thermal insulation and an on/off switch.

Numerical model of an initial-boundary value problem for the system with lossy side thermal insulation

In order to obtain the numerical model of initial-boundary value problem the implicit finite difference method was applied [14]. Model of electrical floor heater presented in Fig. 1 was covered with rectangular mesh nodes of finite difference method. Fragment of this mesh is shown in Fig. 2.

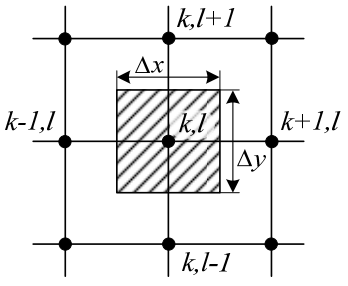

Fig.2. Fragment of mesh nodes of finite difference method with marked control surface

Equation (1) was discretized in time and space. Spatial derivatives of the second-order were approximated with central difference quotients, while the first-order time derivative was replaced with a forward difference quotient. After assuming equal mesh size $(\Delta x = \Delta y)$ and making necessary transformations, differential form of the transient heat equation was obtained:

(13) $$\left(1 + 4Fo_i\right)T_{k,l}^{n+1} - Fo_i\left(T_{k+1,l}^{n+1} + T_{k-1,l}^{n+1} + T_{k,l+1}^{n+1} + T_{k,l-1}^{n+1}\right) = T_{k,l}^{n} + \frac{g_i(\Delta x)^2 Fo_i}{\lambda_i}.$$

In the above equation, subscripts (k,l) denote the location of a node in the finite difference mesh, n is a consecutive time moment and Fo_i denotes Fourier's number corresponding to the ith material:

(14) $$Fo_i = \frac{\chi_i \Delta t}{(\Delta x)^2},$$

where Δt is a time step.

Dimensions of control surface in numerical modelling of the heating cable result from the finite difference mesh size (Fig. 2). This surface area is a square characterized by Δx side (because $\Delta x = \Delta y$). The axis of the cable is in the centre of the square. Volumetric efficiency of the heat source corresponding to the control surface equals:

(15) $$g_{cab} = \frac{Q_{cab}}{\Delta x \Delta y},$$

where Q_{cab} is a linear density of emitted power (W/m).

The heat sources are controlled by a regulator in a manner described in a previous section. Equations (10) take the following form:

(16)
$$g = \begin{cases} g_{cab} \ for \ \{(k,l) \in S_{cab}\} \cap \left[\{n = 0\} \cup \left\{T_C^n \leq T_{ON} \cap T_C^{n+1} < T_C^n\right\}\right] \\ 0 \quad for \ \{(k,l) \in S_{cab}\} \cap \left\{T_C^n \geq T_{OFF}\right\} \cap \left\{T_C^{n+1} > T_C^n\right\} \\ 0 \quad for \ (k,l) \notin S_{cab} \end{cases}$$

where T_C^n is a temperature determined for the nth time step in point C (Fig. 1), in which temperature sensor is located.

Equation (13) may be applied for nodes located inside the analysed model, which are surrounded by four neighbouring nodes. For nodes located on boundaries of the analysed model or on the boundaries of the materials other equations should be introduced. These equations should take boundaries conditions into consideration. For the case of:

- surfaces exchanging heat with environment (Γ_2, Γ_3, Γ_5, Γ_6),
- adiabatic contours (Γ_4, Γ_7, Γ_8, Γ_9),
- boundaries of materials (Γ_{12}, Γ_{14}, Γ_{15}, Γ_{23}, Γ_{25}, Γ_{35}, Γ_{45}),
- corner nodes joining adiabatic contour with a contour of heat transfer ($\Gamma_3 \cap \Gamma_4$, $\Gamma_6 \cap \Gamma_7$),
- corner nodes joining boundary of materials with adiabatic surface ($\Gamma_7 \cap \Gamma_8 \cap \Gamma_{23}$, $\Gamma_8 \cap \Gamma_9 \cap \Gamma_{12}$)

appropriate relations have been derived and presented in [13]. For this purpose, in that paper, the elimination of non-existing nodes [9] or energy balance method was applied [14]. Herein energy balance method was also applied in order to determine equations for the rest of corner nodes. In case of nodes joining boundary of materials with surface of heat transfer, the following equations were obtained:

$$\left(4\lambda_1+4\lambda_4+4\alpha_2\Delta x+\frac{\lambda_1}{Fo_1}+\frac{\lambda_4}{Fo_4}\right)T_{k,l}^{n+1}-2\lambda_1T_{k,l-1}^{n+1}$$

$$-2\lambda_4T_{k,l+1}^{n+1}-2(\lambda_1+\lambda_4)T_{k+1,l}^{n+1}=\left(\frac{\lambda_1}{Fo_1}+\frac{\lambda_4}{Fo_4}\right)T_{k,l}^{n}+4\alpha_2\Delta xT_{amb2}\quad for\ \ \Gamma_2\cap\Gamma_3\cap\Gamma_{14},\tag{17a}$$

$$\left(4\lambda_3+4\lambda_5+4\alpha_1\Delta x+\frac{\lambda_3}{Fo_3}+\frac{\lambda_5}{Fo_5}\right)T_{k,l}^{n+1}-2\lambda_3T_{k+1,l}^{n+1}$$

$$-2\lambda_5T_{k-1,l}^{n+1}-2(\lambda_3+\lambda_5)T_{k,l-1}^{n+1}=\left(\frac{\lambda_3}{Fo_3}+\frac{\lambda_5}{Fo_5}\right)T_{k,l}^{n}+4\alpha_1\Delta xT_{amb1}\quad for\ \ \Gamma_5\cap\Gamma_6\cap\Gamma_{35}.\tag{17b}$$

In contrast, the equation appropriate for the node located on the boundary of materials, which also joins adiabatic contour with contour that gives up the heat to the room, take the following form:

$$\left(4\lambda_4+4\lambda_5+2\alpha_1\Delta x+\frac{\lambda_4}{Fo_4}+\frac{\lambda_5}{Fo_5}\right)T_{k,l}^{n+1}-2\lambda_4T_{k-1,l}^{n+1}$$

$$-2\lambda_5T_{k+1,l}^{n+1}-2(\lambda_4+\lambda_5)T_{k,l-1}^{n+1}=\left(\frac{\lambda_4}{Fo_4}+\frac{\lambda_5}{Fo_5}\right)T_{k,l}^{n}+2\alpha_1\Delta xT_{amb1}\quad for\ \ \Gamma_4\cap\Gamma_5\cap\Gamma_{45}.\tag{18}$$

Equations appropriate for nodes forming the boundary between three materials take other form:

$$\left(8\lambda_1+4\lambda_2+4\lambda_5+\frac{2\lambda_1}{Fo_1}+\frac{\lambda_2}{Fo_2}+\frac{\lambda_5}{Fo_5}\right)T_{k,l}^{n+1}-4\lambda_1T_{k,l-1}^{n+1}$$

$$-2(\lambda_2+\lambda_5)T_{k,l+1}^{n+1}-2(\lambda_1+\lambda_5)T_{k-1,l}^{n+1}-2(\lambda_1+\lambda_2)T_{k+1,l}^{n+1}=\left(\frac{2\lambda_1}{Fo_1}+\frac{\lambda_2}{Fo_2}+\frac{\lambda_5}{Fo_5}\right)T_{k,l}^{n}\quad for\ \ \Gamma_{12}\cap\Gamma_{15}\cap\Gamma_{25},\tag{19a}$$

$$\left(8\lambda_1+4\lambda_4+4\lambda_5+\frac{2\lambda_1}{Fo_1}+\frac{\lambda_4}{Fo_4}+\frac{\lambda_5}{Fo_5}\right)T_{k,l}^{n+1}-4\lambda_1T_{k,l-1}^{n+1}$$

$$-2(\lambda_4+\lambda_5)T_{k,l+1}^{n+1}-2(\lambda_1+\lambda_4)T_{k-1,l}^{n+1}-2(\lambda_1+\lambda_5)T_{k+1,l}^{n+1}=\left(\frac{2\lambda_1}{Fo_1}+\frac{\lambda_4}{Fo_4}+\frac{\lambda_5}{Fo_5}\right)T_{k,l}^{n}\quad for\ \ \Gamma_{14}\cap\Gamma_{15}\cap\Gamma_{45},\tag{19b}$$

$$\left(4\lambda_2+4\lambda_3+8\lambda_5+\frac{\lambda_2}{Fo_2}+\frac{\lambda_3}{Fo_3}+\frac{2\lambda_5}{Fo_5}\right)T_{k,l}^{n+1}-4\lambda_5T_{k-1,l}^{n+1}$$

$$-2(\lambda_2+\lambda_3)T_{k+1,l}^{n+1}-2(\lambda_3+\lambda_5)T_{k,l+1}^{n+1}-2(\lambda_2+\lambda_5)T_{k,l-1}^{n+1}=\left(\frac{\lambda_2}{Fo_2}+\frac{\lambda_3}{Fo_3}+\frac{2\lambda_5}{Fo_5}\right)T_{k,l}^{n}\quad for\ \ \Gamma_{23}\cap\Gamma_{25}\cap\Gamma_{35}.\tag{19c}$$

On the bottom surface of concrete base (Γ_1) nodes have a constant temperature T_g.

Differential equations written for all nodes of finite difference mesh form a system of linear algebraic equations. The number of unknowns present in this system (i.e. temperature values in nodes of the mesh) is $K\cdot(L-1)$, where K is the number of the nodes in direction of the x axis, and L is the number of nodes in direction of y axis.

The temperature of all nodes of the model at the initial moment of time $n = 0$ (i.e. in steady state before turning on the power) has to be determined in order to begin numerical calculations of transient state of the working floor heating system. To determine these values, new differential equations for the model with switching off the heating cable should be obtained. Changes result from fundamental differences between parabolic (1) and elliptic (11) equations.

During the discretization of equation (11) second-order derivatives were replaced with the central difference quotients. This resulted in the following equation applicable for nodes located inside the model:

$$T_{k+1,l}+T_{k-1,l}+T_{k,l+1}+T_{k,l-1}-4T_{k,l}=0.\tag{20}$$

In contrast nodes located on outer boundaries of the model or on boundaries of materials require derivation of new equations concerning boundary conditions. As in the case of transient state, most of the dependences were presented in [13]. Energy balance method was applied to obtain the rest of the equations. In case of nodes joining boundary of materials with surface of heat transfer the following equations were obtained:

$$-2(\lambda_1+\lambda_4+\alpha_2\Delta x)T_{k,l}+(\lambda_1+\lambda_4)T_{k+1,l}+\lambda_1T_{k,l-1}+\lambda_4T_{k,l+1}=-2\alpha_2\Delta xT_{amb2}\quad for\quad\Gamma_2\cap\Gamma_3\cap\Gamma_{14},\tag{21a}$$

$$-2(\lambda_3+\lambda_5+\alpha_1\Delta x)T_{k,l}+(\lambda_3+\lambda_5)T_{k,l-1}+\lambda_3T_{k+1,l}+\lambda_5T_{k-1,l}=-2\alpha_1\Delta xT_{amb1}\quad for\quad\Gamma_5\cap\Gamma_6\cap\Gamma_{35}.\tag{21b}$$

while in the case of the node located on the boundary of materials and joining adiabatic edge with a contour of heat transfer, the following equation was derived:

$$-(2\lambda_4+2\lambda_5+\alpha_1\Delta x)T_{k,l}+(\lambda_4+\lambda_5)T_{k,l-1}+\lambda_4T_{k-1,l}+\lambda_5T_{k+1,l}=-\alpha_1\Delta xT_{amb1}\quad for\quad\Gamma_4\cap\Gamma_5\cap\Gamma_{45}.\tag{22}$$

Next equations apply to nodes located on boundaries of three materials:

$$-2(2\lambda_1+\lambda_2+\lambda_5)T_{k,l}+(\lambda_2+\lambda_5)T_{k,l+1}+(\lambda_1+\lambda_2)T_{k+1,l}+(\lambda_1+\lambda_5)T_{k-1,l}+2\lambda_1T_{k,l-1}=0\quad for\quad\Gamma_{12}\cap\Gamma_{15}\cap\Gamma_{25},\tag{23a}$$

$$-2(2\lambda_1+\lambda_4+\lambda_5)T_{k,l}+(\lambda_4+\lambda_5)T_{k,l+1}+(\lambda_1+\lambda_5)T_{k+1,l}+(\lambda_1+\lambda_4)T_{k-1,l}+2\lambda_1T_{k,l-1}=0\quad for\quad\Gamma_{14}\cap\Gamma_{15}\cap\Gamma_{45},\tag{23b}$$

$$-2(2\lambda_2+\lambda_3+2\lambda_5)T_{k,l}+(\lambda_3+\lambda_5)T_{k,l+1}+(\lambda_2+\lambda_3)T_{k+1,l}+(\lambda_2+\lambda_5)T_{k,l-1}+2\lambda_5T_{k-1,l}=0\quad for\quad\Gamma_{23}\cap\Gamma_{25}\cap\Gamma_{35}.\tag{23c}$$

Writing differential equations of steady state for subsequent nodes, the system of linear algebraic equations is obtained. The solution of this system of equations is the initial condition for the system of equations corresponding to transient state of the heater.

Software and parameters of the model of a heater

In case of analysed electrical floor heater with lossy side thermal insulations (Fig. 1), following dimensions of the model were taken into consideration:

$$d_1=0.15\,m,\ d_2=0.1\,m,\ d_3=0.08\,m,\ d_{cab}=0.06\,m,\ w_1=1.83\,m,\ w_2=1.54\,m,\ w_4=0.26\,m,\ w_5=0.03\,m,\ w_c=0.56\,m,\ w_{cab}=0.14\,m.\tag{24}$$

In case of the system with ideal side thermal insulation, the same dimensions of the model were taken into consideration, but the analysis was limited to hatched area shown in Fig. 1.

It is assumed that the slab and the base are made of concrete characterised by the same parameters. What is more, it is assumed that basic and side thermal insulations are made of the same foamed polystyrene. Parameters of the materials, from which parts of the heater are made of, are presented in Table 1.

Table 1. Material parameters of the floor heater model

Parameter	Symbol [unit]	Material i		
		1 and 3	2 and 5	4
Thermal conductivity	λ_i $[W/(m \cdot K)]$	1.0	0.04	0.77
Specific heat	c_i $[J/(kg \cdot K)]$	840	1460	880
Mass density	ρ_i $[kg/m^3]$	2000	20	1800

The following additional parameters were used during the simulation of the floor heater:

$$\begin{aligned} &T_{amb1} = 14°C,\ \alpha_1 = 9\ W/(m^2 \cdot K),\ T_{ON} = 25.5°C, \\ &T_{amb2} = 14°C,\ \alpha_2 = 7\ W/(m^2 \cdot K),\ T_{OFF} = 26.5°C, \\ &T_g = 10°C,\ Q_{cab} = 20\ W/m. \end{aligned} \tag{25}$$

The analysed model of the heater was covered with a finite difference mesh of the size $\Delta x = \Delta y = 0.0025\ m$. The mesh consisted of $K = 733$ nodes in the direction of x axis and $L = 133$ nodes in the direction of y axis. Because of known temperature values of nodes located at contour Γ_1, the total number of unknowns (in each system of linear algebraic equations) was 96 756. In order to determine the initial temperature field distribution, the system of equations resulting from the differential form (11) and appropriate boundary conditions, had to be solved one time. However the analysis of the transient state consists of solving (multiple times, for consecutive time moments $n = 1, 2, ...$) system of equations resulting from a differential form of the problem (1)-(10), (12). The operation of a floor heater during 24 h from the system start up was analysed. Application of time step $\Delta t = 2\ s$ required the execution of 43 200 steps of the calculation method.

In order to solve systems of equations and determine the transient state temperature field distribution author's computer program was developed in C++ language. Because the coefficients matrices of obtained systems of equations contained a very small number of non-zero elements, they were stored in a computer memory with the use of CSR (Compressed Sparse Row) method [11, 12]. Systems of equations were solved with the use of Biconjugate Gradient Stabilized method (BiCGStab) with Jacobi preconditioner. In order to shorten the computation time, the algorithm of this method was implemented on a GPU, which assists traditional processor (CPU). For that reason Nvidia's CUDA parallel computing platform [15, 16] and two bundled linear algebra libraries - CUBLAS [17] and CUSPARSE [18] - were applied. The computations were carried out with the use of a personal computer equipped with the Intel Core 2 Quad CPU Q9650 3.00 GHz processor, 4 GB RAM memory and Gigabyte Nvidia GeForce GTX480 graphic card (480 CUDA cores, 1536 MB of GDDR5 memory). The program was executed under Microsoft Windows 7 Professional operating system.

Influence of lossiness of side insulation on thermal field distribution of the heater

As a result of numerical computations, transient temperature field distributions of two analysed models (with ideal and lossy side thermal insulation) were obtained. Comparison of temperature distributions on the surface of the floor after a specified period of time from supplying power to heating cable (contour Γ_6, Fig. 1) is presented in Fig. 3. In case of the system with lossy side thermal insulation temperature values in all nodes of the model directly result from calculations. However, in case of a system with ideal side thermal insulation, the calculations were only carried out for the area of the floor hatched in Fig. 1 (distance from 0.29 m to 0.36 m in Fig. 3). In more distant parts of the section of the floor (distance from 0.36 m up to 0.43 m) the temperature field distribution is a mirror image of distribution described earlier. In subsequent segments it is repeated every 0.14 m. Such field distribution is forced by adiabatic planes occurring in the model with ideal side thermal insulation.

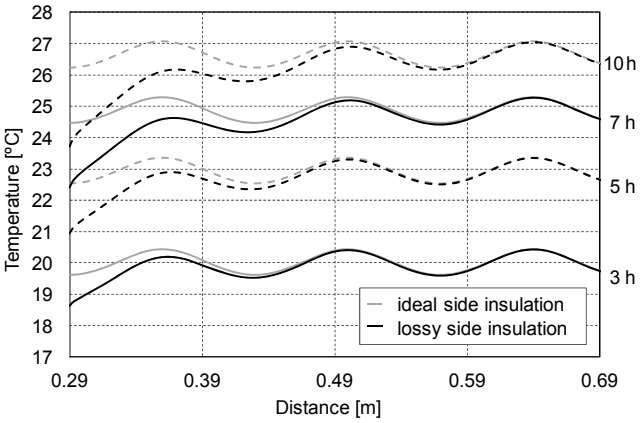

Fig.3. Temperature distribution on the surface of the floor in selected time steps

Analysing Fig. 3 it can be seen that the temperature of points located near the left edge of the floor (x = 0.29 m) is lower in the model with a lossy side thermal insulation than in the model with perfect side insulation. This is caused by a part of the heat flux passing through a lossy side insulation towards the outer wall, causing a decrees of the temperature of this part of the floor. Towards the centre of the floor, the differences between the temperatures in two models decrease, and from about 0.59-0.69 m temperatures are equal. Loss of heat through sides of heater also causes displacement of extreme temperature points. In the model with ideal side insulation points of the highest temperature on the surface of the floor were located directly above sections of the heating cable. Points of the lowest temperature on the surface of the floor were located in the middle of the distance between them. In the model with lossy side insulation points of maximum temperature are shifted to the right (first maximum is shifted by 0.015 m and second is shifted by 0.005 m). In contrast, points of minimal temperature are shifted to the left (first minimum is shifted by 0.01 m and second is shifted by 0.0025 m). With the passing of time, the temperature difference between adiabatic case and real case increases (Fig. 3, for $0.29 \le x < 0.59$ m). This phenomenon is caused by the increase of concrete slab temperature. Increase of this temperature forces greater heat loss to the environment.

Temperature profile (relationship between time and temperature) of two selected points located on the surface of the floor - A and B (Fig. 1) - is presented in Fig. 4. Two specific periods are distinguished in the operation of the floor heater. During the first period, the transient state occurs. In this state the profile is aperiodic (i.e. there is no oscillation). In both models, transient states last for approximately 10.6 hours. In the second period system works with an on/off controller operating with a sensor, which abscissa is $x_c = w_4 + w_5 + w_c$ = 0.85 m > 0.69 m. At

this point, the temperature profiles are almost the same in both adiabatic and real cases (Fig. 3). Therefore, the operation of turning on the power of the heating cable and the operation of turning it off are conducted at a similar time (time difference does not exceed 1 minute). In the case of model with ideal thermal side insulation the temperatures of points A and B are higher than in the case of lossy model. In both models the temperature of point B (located above the cable) is higher than the temperature of point A. System with adiabatic side insulation warms up faster (e.g. point B reaches 26 ºC 1.7 h earlier).

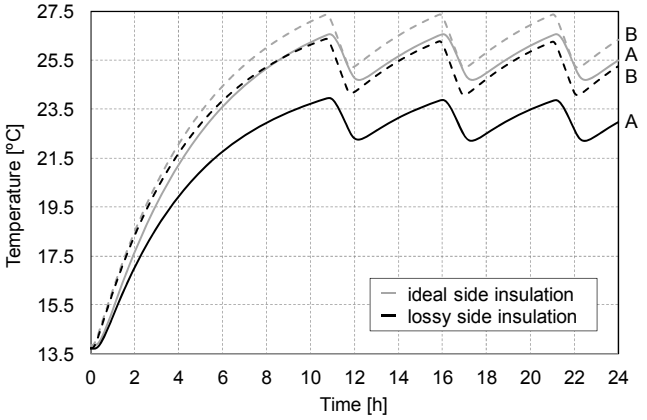

Fig.4. Temperature profile of selected heater points (A and B)

Fig. 5 shows the temperature distribution over the half of the surface of the floor at the moment of the first turning off the power of the heating cable (OFF) and at the moment of turning it on again (ON). Drop of temperature at the left edge of the floor is clearly noticeable in case of the model with lossy side thermal insulation. In the outermost left point differences between models reach up to 2.5 °C.

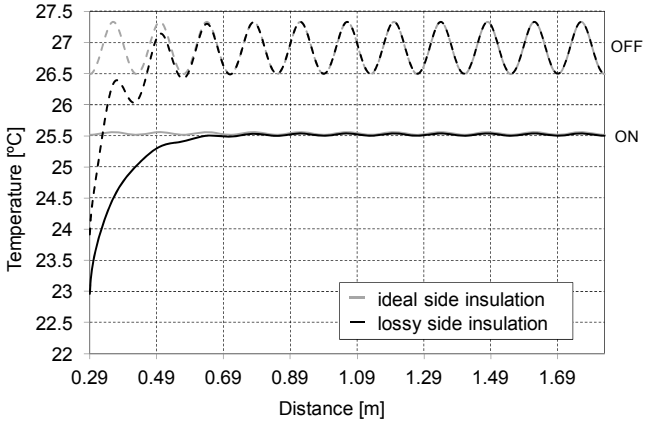

Fig.5. Temperature distribution on the surface of the floor at the moment of the first turning off the power of the heating cable (OFF) and at the moment of turning it on again (ON)

Influence of modelling lossiness of side insulation on the numerical computations

Method of modelling side thermal insulation significantly affects the size of analysed model of an electrical floor heating system. In case of a system with perfect side insulation, computations are carried out only for half of repeatable floor segment (hatched area in Fig. 1). Whereas, in case of the system with lossy side insulation, the temperature distribution is computed for the whole model presented in Fig. 1. This increases **26 times** the number of unknowns and the number of non-zero elements of the coefficient matrix (in comparison with model with adiabatic side insulation). Discussed parameters of the model with lossy side insulation are collected in Table 2 (for 4 sizes of the finite difference mesh).

Table 2. Division of floor heater model and parameters of the system of equations (lossy side thermal insulation)

Mesh size Δx [m]	Mesh	Number of unknowns	Number of non-zero elements of the coefficient matrix
0.0025	733 × 133	96 756	482 050
0.00125	1465 × 265	386 760	1 930 342
0.000625	2929 × 529	1 546 512	7 725 646
0.0003125	5857 × 1057	6 184 992	30 911 134

Increased size of solved systems of equations significantly increases execution time of the program modelling lossy side insulation: the program is executed at least 2 times longer (for step size Δx = 0.0025 m) and up to about 16 times longer (for step size Δx = 0.0003125 m) in comparison with program modelling ideal side insulation. Detailed summary is presented in Table 3.

Table 3. Ratio of execution time of models with lossy and with adiabatic insulation

Mesh size Δx [m]	Execution time of a model with lossy side insulation [s]	Ratio of execution time of models with lossy and adiabatic side insulation
0.0025	176.42	2.22
0.00125	777.31	4.68
0.000625	3 838.01	9.39
0.0003125	24 551.20	16.47

Times presented in Table 3 were obtained by conducting simultaneous calculations on CPU and GPU. Comparison of these times with times of programs executed only on traditional CPU is interesting. Because of that, sequential versions of programs for models with ideal and lossy side insulation were created. In these programs, algorithm of BiCGStab method was implemented with the use of Intel Math Kernel Library (MKL) [19] - a library containing a set of procedures for numerical linear algebra. Speed-ups were calculated on the basis of obtained execution times. Speed-up was defined as the ratio of time of execution of the program only on traditional processor (t_{CPU}) and time of execution of the program on traditional processor and graphics processor unit ($t_{CPU+GPU}$) [20]:

$$S = \frac{t_{CPU}}{t_{CPU+GPU}}. \tag{26}$$

Obtained times and speed-up values are presented in Table 4.

Table 4. Speed-up in the model with lossy and ideal side thermal insulation

Mesh size Δx [m]	Execution time of a model with lossy side insulation		Speed-up in a model with lossy side insulation	Speed-up in a model with ideal side insulation
	CPU [s]	CPU+GPU [s]		
0.0025	590.34	176.42	3.35	0.33
0.00125	5 632.73	777.31	7.25	0.68
0.000625	45 200.73	3 838.01	11.78	1.86
0.0003125	366 145.37	24 551.2	14.91	7.54

In the system with ideal side insulation additional application of the GPU reduced the computation time only in cases of two the most dense meshes. Whereas, in the system with lossy side insulation the speed-up was obtained in all cases. The speed-up ranged from 3.35 to 14.91. Larger speed-ups obtained in cases of models with lossy side insulation are caused by larger systems of linear algebraic equations. Such systems of equations allow a better utilization of the GPU computing power.

Final remarks

Comparison of two models of electrical floor heating systems (system with ideal side thermal insulation and system with lossy side thermal insulation) were presented in this paper. Author's software was developed. This software enabled determining the distribution of transient temperature field in the cross-section of a heater. Programs used parallel computations performed simultaneously on a CPU and a GPU. It has been found that taking lossy side thermal insulation into consideration has the greatest influence on temperature field distribution in the edge layer. The deformation of the temperature field distribution appearing in this area reaches its maximum at the left edge of the floor and decays after the distance of approximately 0.3-0.4 m towards the centre of the floor (Fig. 3). In addition, temperature extremes change their locations. In comparison with a model with ideal side thermal insulation, maxima are shifted to the right and the minima are shifted to the left. Model of side thermal insulation has no impact on work cycles of on/off controller. This is caused by the position of temperature sensor (it is located outside of the area in which the temperature decrease appears in case of model with lossy side insulation).

Taking lossy side thermal insulation into account causes a significant increase of the size of analysed model of a floor heater, thus there is a grow of number of nodes of finite difference mesh and the number of unknowns in solved systems of equations. This significantly extends the time of the analysis. The paper shows that the application of GPU shortens the time of computations.

The paper was prepared at Bialystok University of Technology within a framework of the S/WE/01/2013 project sponsored by the Ministry of Science and Higher Education.

***Autorzy**: prof. dr hab. inż. Jerzy Gołębiowski, Politechnika Białostocka, Wydział Elektryczny, ul. Wiejska 45D, 15-351 Białystok, E-mail: j.golebiowski@pb.edu.pl; dr inż. Jarosław Forenc, Politechnika Białostocka, Wydział Elektryczny, ul. Wiejska 45D, 15-351 Białystok, E-mail: j.forenc@pb.edu.pl.*

LITERATURA

[1] Patankar S.V., *Numerical Heat Transfer and Fluid Flow*, McGraw Hill Book Company, New York, (1980).
[2] Woodson R.D., *Radiant Floor Heating, Second Edition*, McGraw-Hill, New York, (2009).
[3] Żukowski M., *Ogrzewanie podłogowe*, Oficyna Wydawnicza Politechniki Białostockiej, Białystok, (2009).
[4] Laouadi A., Development of a radiant heating and cooling model for building energy simulation software, *Building and Environment*, 39 (2004), No. 4, 421-431.
[5] Holopainen R., Tuomaala P., Piippo J., Uneven gridding of thermal nodal networks in floor heating simulations, *Energy and Buildings*, 39 (2007), No. 10, 1107-1114.
[6] Jin X., Zhang X., Luo Y., A calculation method for the floor surface temperature in radiant floor system, *Energy and Buildings*, 42 (2010), No. 10, 1753-1758.
[7] Larsen S.F., Filippín C., Lesino G., Transient simulation of a storage floor with a heating/cooling parallel pipe system, *Building Simulation*, 3 (2010), No. 2, 105-115.
[8] Liu Y., Wang D., Liu J., Study on heat transfer process for in-slab heating floor, *Building and Environment*, 54 (2012), 77-85.
[9] Gołębiowski J., Forenc J., Parallel computations of the step response of a floor heater with the use of a graphics processing unit. Part 1: Models and algorithms, *Bull. Pol. Ac.: Tech.*, 61 (2013), No. 4, 943-948.
[10] Van der Vorst H., Bi-CGSTAB: A fast and smoothly converging variant of Bi-CG for the solution of nonsymmetric linear systems, *SIAM J. Sci. and Stat. Comput.*, 13 (1992), No. 2, 631-644.
[11] Barrett R., Berry M., Chan T.F., Demmel J., Donato J.M., Dongarra J., Eijkhout V., Pozo R., Romine Ch., Van der Vorst H., *Templates for the Solution of Linear Systems: Building Blocks for Iterative Methods*, SIAM, Philadelphia, (1994).
[12] Saad Y., *Iterative Methods for Sparse Linear Systems, Second Edition*, SIAM, (2003).
[13] Forenc J., Analiza niestacjonarnego pola temperatury elektrycznego grzejnika podłogowego z wykorzystaniem procesora karty graficznej, *Przegląd Elektrotechniczny*, 91 (2015) nr. 9, 282-289.
[14] Incropera F., De Witt D., Bergman T., Lavine A., *Fundamentals of Heat and Mass Transfer*, John Wiley & Sons, Hoboken, (2007).
[15] Cook S., *CUDA Programming. A Developer's Guide to Parallel Computing with GPUs*, Morgan Kaufmann, Amsterdam, (2013).
[16] Cheng J., Grossman M., McKercher T., *Professional CUDA C Programming*, Wrox, 2014.
[17] CUBLAS Library, User Guide, NVIDIA Corporation, Santa Clara, CA, (2013).
[18] CUSPARSE Library, NVIDIA Corporation, Santa Clara, CA, (2013).
[19] Intel Math Kernel Library. Reference Manual, MKL 10.3 Update 10, Intel Corporation, (2012).
[20] Jalili-Marandi V., Dinavahi V., SIMD-based large-scale transient stability simulation on the graphics processing unit, *IEEE Trans. on Power Systems*, 25 (2010), No. 3, 1589-1599.